JOURNAL OF GUIDANCE, CONTROL, AND DYNAMICS
Vol. 29, No. 3, May–June 2006

Dynamics and Control of Displaced Periodic Orbits Using Solar-Sail Propulsion

John Bookless*
University of Glasgow, Glasgow, Scotland G12 8QQ, United Kingdom
and
Colin McInnes†
University of Strathclyde, Glasgow, Scotland G1 1XJ, United Kingdom

Solar-sail propulsion to generate families of displaced periodic orbits at planetary bodies is considered. These highly non-Keplerian orbits are achieved using the constant acceleration from the solar sail to generate an artificial libration point, which then acts as a generator of periodic orbits. The orbit is modeled first using two-body and then three-body dynamics including solar radiation pressure effects. A two-body stability condition for the orbits is derived using both a linear and nonlinear analysis and a Jacobi-type integral to identify zero-velocity surfaces that bound the orbital motion. A new family of highly perturbed orbits is then identified resulting in a set of useful manifolds, which can be used for orbit insertion. A closed-form solution to the two-body case is derived using parabolic coordinates, which allows separation of the Hamiltonian of the problem. It is demonstrated that the manifolds are bound to the surface of a paraboloid. A three-body analysis is performed by using Hill's equations as an approximation to the circular restricted three-body problem. Stationkeeping techniques are also investigated to prevent escape after arrival at the desired highly non-Keplerian orbit.

Nomenclature

$\boldsymbol{a}$, A	=	solar-sail acceleration, state transition matrix
B	=	control matrix
C	=	output matrix
E	=	total energy
G	=	gain matrix
H, h_z	=	two-body Hamiltonian, z component of angular momentum
L_s, L	=	solar luminosity, central body radius
M	=	performance matrix
M_c, M_o	=	controllability matrix, observability matrix
$\boldsymbol{n}$, N	=	solar-sail normal vector, control-weighting matrix
P_g	=	momentum relative to the g axis
Q, δQ	=	state weighting matrix, perturbation vector
R, r	=	sun–sail distance, Earth-sail distance
T	=	kinetic energy
U	=	potential energy
v	=	solar-sail velocity
z, δz	=	sun-line displacement distance, applied displacement perturbation
α, $\delta\alpha$	=	pitch angle, pitch-angle variation
β	=	solar-sail lightness number
θ	=	angular position around sun line
κ, $\delta\kappa$	=	nondimensionalized sail acceleration, sail acceleration variation
λ	=	eigenvalues from characteristic equation
μ_s, μ	=	sun gravitational parameter, Earth gravitational parameter
ξ, η	=	parabolic coordinates
ρ, $\delta\rho$	=	orbit radius, applied radial perturbation
σ	=	sail loading parameter
τ	=	characteristic time
χ	=	control parameter
ψ	=	Cartesian pitch angle
ϕ, Φ	=	Cartesian yaw angle, separation constant

Received 21 January 2005; revision received 14 April 2005; accepted for publication 18 April 2005.

*Research Student, Department of Aerospace Engineering.
†Professor, Department of Mechanical Engineering.

Introduction

SOLAR sailing is an emerging form of propulsion that exploits solar radiation pressure to provide thrust. The sail is a tensioned thin reflective film with a thickness of order 1 μm and with a large area. A key advantage of solar sails over conventional propulsion systems is that missions are not constrained by the Δv available from stored reaction mass. This enables many new and exciting high-energy mission concepts. Several authors including Dachwald and Seboldt,[1] Seboldt and Dachwald,[2] Leipold and colleagues,[3,4] Hughes et al.,[5] and Macdonald and McInnes[6] have demonstrated that solar-sail propulsion would enable planetary and small-body sample returns that require large Δv. McInnes and coworkers,[7–9] Forward,[10] and Morrow et al.[11] have demonstrated that solar sails can be used to provide a constant thrust that can generate artificial libration points in the circular restricted three-body problem. These artificial equilibria are of interest because the solar sail is being used to provide new vantage points for observation, rather than as an efficient means of transferring payloads between orbits.

Displaced non-Keplerian orbits at planetary bodies can be achieved by orientating the solar sail normal to the sun line. The constant acceleration generated by the solar sail then forms an artificial libration point, which can generate families of periodic orbits.[12,13] In this paper, the dynamics of these orbits will be investigated using two-body dynamics. A linear and nonlinear analysis will be used to investigate the stability of these orbits. Energy methods can then be applied to identify zero-velocity surfaces, which determine long-term orbit stability. It is shown that a new family of highly perturbed orbits can be generated by applying a small perturbation to the nominal sail acceleration. The resulting trajectory winds off the nominal orbit and then performs a loop about the central body before returning to the nominal orbit. In principle, this provides a set of invariant manifolds exhibiting homoclinic connection. As will be seen, these manifolds can be used for insertion from low Earth orbit onto a displaced non-Keplerian orbit with reduced Δv requirements. A closed-form solution can be derived by converting the two-body equations of motion to parabolic coordinates (the so-called Stark problem).[14] It is demonstrated that this highly perturbed family of orbits is in fact bound to the surface of a paraboloid. The

parabolic bounding surfaces can be used to identify the closest approach to the central body, and the required insertion conditions can be determined.

After insertion to a displaced non-Keplerian orbit, station-keeping techniques are required to prevent the solar sail escaping from the final (unstable) orbit. Two possible techniques that can be used to actuate control are sail area variation and sail pitch-angle variation. A controllability and observability matrix will be examined to ensure both methods provide full controllability. A linear controller is designed and the gains selected to position the transfer-function poles to suppress positive real eigenvalues.

An improvement to the two-body model is achieved by using Hill's approximation to the circular restricted three-body problem to model the families of non-Keplerian orbits. The acceleration due to solar radiation pressure will also include the inverse square dependency of solar radiation pressure on sun-sail distance. To prevent escape after orbit insertion, solar-sail stationkeeping techniques are again employed. The two-body controller can be adapted to control the three-body non-Keplerian orbit. A linear quadratic regulator (LQR) is designed to enable optimal control gains to be selected.

Finally, displaced periodic orbits could be used to position a science payload permanently within the geomagnetic tail. A possible mission, which could provide a long-term survey of the geomagnetic tail and provide insights into the reconnection processes occurring within the geomagnetic tail, is investigated. The region of interest is located $\sim 30\ R_E$ (Earth radii) from the Earth, in the antisun direction. The transfer Δv requirements are calculated for each stage of orbit insertion.

Solar Sails

Solar sails consist of large-area gossamer structures with a reflective coating that intercepts a flux of solar photons. Photons incident on the sail impart momentum, and the reflection results in a reaction force, thus providing double the force that would be imparted to an absorbing surface. For an ideal sail, the total thrust is normal to the sail surface. Because solar sails do not rely upon the expulsion of stored reaction mass to generate thrust, they can theoretically maintain continuous acceleration, allowing new families of highly non-Keplerian orbits.[7,12,13,15,16] Solar sails could also enable many high energy missions including planetary sample return,[5] multiple near-Earth asteroid[1] rendezvous, or solar polar orbiter.[17]

The solar-sail acceleration is dependent on its areal density, also known as the sail loading parameter. The sail acceleration $\boldsymbol{a}$ is then defined by

$$\boldsymbol{a} = \left(\beta \mu_s \big/ R^2\right) \cos^2 \alpha \boldsymbol{n} \tag{1}$$

where α is the angle of the sail normal vector $\boldsymbol{n}$ to the sun line (pitch angle) and β is the solar-sail lightness number, defined as the ratio of solar radiation pressure to gravitational acceleration[15] so that

$$\beta = L_s / 2\pi c \mu_s \sigma \tag{2}$$

where c is the speed of light, and σ is the ratio of solar-sail mass to surface area, the sail loading parameter. Because both solar gravity and solar radiation pressure have an inverse square variation with heliocentric distance, the sail lightness number is a fixed parameter for a solar sail with a given loading.

Displaced Non-Keplerian Orbits

A solar sail is considered in orbit about a planet (ignoring the higher harmonics of the gravitational potential). By orientating the solar sail normal to the sun line ($\alpha = 0$), the constant acceleration generated can be used to create a circular non-Keplerian orbit, displaced from the central body in the antisun direction, as shown in Fig. 1.[12,13] The solar-sail dynamics can initially be modeled using the two-body problem, where the two-body Hamiltonian $H = T + U$. These can be represented using polar coordinates (ρ, z, θ), where the z axis is parallel to the sun line and ρ is the orbit radius so that

$$T = \tfrac{1}{2}(\dot{z}^2 + \dot{\rho}^2 + \rho^2 \dot{\theta}^2) \tag{3a}$$

$$U = -\mu/r - az \tag{3b}$$

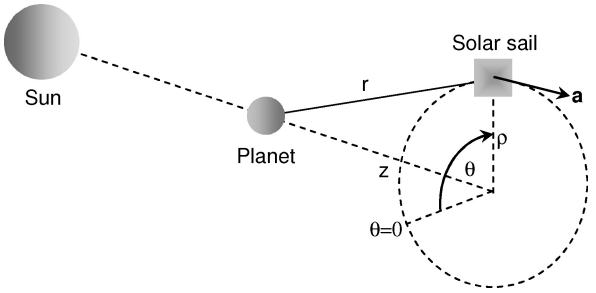

Fig. 1 Schematic of non-Keplerian orbit displaced from the central body in the antisun direction.

and so

$$H = \tfrac{1}{2}\left[P_z^2 + P_\rho^2 + (h_z/\rho)^2\right] - \mu/r - az \tag{3c}$$

where $P_\rho = \partial H / \partial \dot{\rho}$ and $P_z = \partial H / \partial \dot{z}$ are the momenta corresponding to the ρ and z axis and $h_z = \rho^2 \dot{\theta}$ represents the (constant) angular momentum directed along the sun line. The distance between the central body and the solar sail is defined as $r = \sqrt{(\rho^2 + z^2)}$. The acceleration due to solar radiation pressure is represented by a [from Eq. (1)] when the solar sail is orientated normal to the sun line ($\alpha = 0$). The Hamiltonian can be nondimensionalized using a characteristic length $L = 1$ (central body radius) and characteristic time $\tau = \sqrt{(L^3/\mu)}$, where μ is the gravitational parameter of the planet.

The nondimensionalized solar-sail acceleration is now represented by κ, again with a pitch angle $\alpha = 0$, and corresponds to the ratio of the solar radiation pressure induced acceleration to the local gravitational acceleration at unit radius so that $\kappa = aL^2/\mu$. Using the Hamiltonian, $\dot{P}_\rho = -\partial H / \partial \rho$, and $\dot{P}_z = -\partial H / \partial z$, so that the two-body equations of motion can be written as

$$\ddot{\rho} = h_z^2 \big/ \rho^3 - \rho / r^3 \tag{4a}$$

$$\ddot{\theta} = -2\dot{\rho}\dot{\theta}/\rho \tag{4b}$$

$$\ddot{z} = -z/r^3 + \kappa \tag{4c}$$

Equation (4b) can be manipulated again to prove that the z component of angular momentum $h_z = \rho^2 \dot{\theta}$ is conserved, as noted from the Hamiltonian. For a circular orbit with constant displacement distance, the ρ–z velocity and acceleration components $\dot{\rho}$, $\ddot{\rho}$, $\dot{z}$, $\ddot{z}$ are set equal to zero. Equation (4a) then gives the required orbital angular velocity as $\dot{\theta} = r^{-3/2}$, and Eq. (4c) gives the required sail acceleration as $\kappa = z/r^3$. The system possesses a single libration point with $\rho = 0$, and so $\kappa = 1/z^2$. Therefore, for a fixed sail acceleration κ the surface represented by $\kappa = z/r^3$ begins at the origin ($\rho = 0$, $z = 0$) and terminates at $\rho = 0$, $z = 1/\kappa^{1/2}$. For $z < 1/\kappa^{1/2}$ a set of displaced orbits is generated.

Non-Keplerian Orbit Stability

Linear Stability Condition

Equations (4a) and (4c) are represented by the functions $f_\rho(\rho, z) = h_z^2/\rho^3 - \rho/r^3$ and $f_z(\rho, z) = -z/r^3 + \kappa$, respectively. A perturbation can then be defined as $\rho = \rho_0 + \delta\rho$ and $z = z_0 + \delta z$. Using the Taylor expansion, the linearized equations have the form

$$\frac{\mathrm{d}^2(\delta\rho)}{\mathrm{d}t^2} = A_{11}\delta\rho + A_{12}\delta z \tag{5a}$$

$$\frac{\mathrm{d}^2(\delta z)}{\mathrm{d}t^2} = A_{21}\delta\rho + A_{22}\delta z \tag{5b}$$

ignoring higher-order terms, where the notation A_{11}, A_{12}, A_{21}, A_{22} represents the partial derivatives $\partial f_\rho/\partial\rho$, $\partial f_\rho/\partial z$, $\partial f_z/\partial\rho$, and $\partial f_z/\partial z$, respectively, evaluated on the nominal displaced, circular orbit. The partial derivatives are defined as

$$A_{11} = -3h_z^2 \big/ \rho_0^4 - 1 \big/ r_0^3 + 3\rho_0^2 \big/ r_0^5 \tag{6a}$$

$$A_{12} = 3\rho_0 z_0 / r_0^5 = A_{21} \tag{6b}$$

$$A_{22} = -1/r_0^3 + 3z_0^2/r_0^5 \tag{6c}$$

The perturbation terms can be represented by a vector $\delta \boldsymbol{Q} = [\delta\rho, \delta z]^T$ allowing Eqs. (5a) and (5b) to be written in matrix form as

$$\begin{bmatrix} 1 & 0 \\ 0 & 1 \end{bmatrix} \delta\ddot{\boldsymbol{Q}} - \begin{bmatrix} A_{11} & A_{12} \\ A_{21} & A_{22} \end{bmatrix} \delta\boldsymbol{Q} = \begin{bmatrix} 0 \\ 0 \end{bmatrix} \tag{7}$$

For a constant coefficient problem it can be assumed that $|\delta\boldsymbol{Q}| = Q_0 \exp(\lambda t)$, where λ is a constant. Substituting into Eq. (7), the characteristic polynomial is obtained as

$$\lambda^4 - \lambda^2(A_{11} + A_{22}) + \left(A_{11}A_{22} - A_{12}^2\right) = 0 \tag{8}$$

Substituting the constant angular momentum $h_z = \rho_0^2\dot{\theta}$ and the angular velocity $\dot{\theta} = r_0^{-3/2}$ terms into Eq. (6), the partial derivatives can be written in the form $A_{11} = -4\dot{\theta}^2 + 3\dot{\theta}^2\rho_0^2/r_0^2$, $A_{12} = 3\dot{\theta}^2\rho_0 z_0/r_0^2 = A_{21}$, and $A_{22} = -\dot{\theta}^2 + 3\dot{\theta}^2 z_0^2/r_0^2$. If $\lambda^2 > 0$, the orbit is unstable because λ is real, and so $|\delta\boldsymbol{Q}| \to \infty$. For stability, $\lambda^2 < 0$ so that λ is purely imaginary, and so $|\delta\boldsymbol{Q}| \leq Q_0$ (Ref. 16). Equation (8) can be solved for λ^2 to obtain

$$\lambda^2 = -\dot{\theta}^2[(r_0 \pm 3z_0)/r_0] \tag{9}$$

Examining the stability condition, it can be shown that Eq. (9) reduces to $\rho_0 > 2\sqrt{2}z_0$. This is the linear stability condition for a circular, displaced non-Keplerian orbit. This agrees with a stability analysis performed by Dankowicz using Kustaanheimo-Stiefel (KS) variables.[18] Figure 2a represents an example stable orbit ($\rho_0 > 2\sqrt{2}z_0$), whereas Fig. 2b represents an example unstable orbit. Although conditions for linear stability have been found, these are necessary but not sufficient conditions for nonlinear stability. Determining the conditions for nonlinear stability will now require other methods.

Nonlinear Stability Condition

A nonlinear stability condition can be investigated by considering the effective potential of a displaced circular orbit. From the relationship between force and effective potential energy, $\ddot{\rho} = -U_\rho$, and $\ddot{z} = -U_z$, so that a pseudopotential energy function $U(\rho, z)$ can be derived from Eqs. (4a) and (4c) as

$$U(\rho, z) = h_z^2/2\rho^2 - 1/r - \kappa z \tag{10}$$

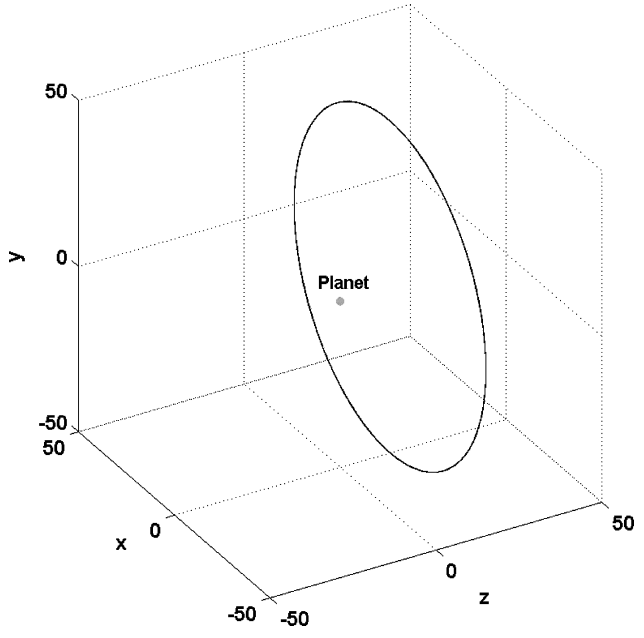

Fig. 2a Stable displaced non-Keplerian orbit ($\rho_0 > 2\sqrt{2}z_0$): $\rho_0 = 50$ L, $z_0 = 15$ L, and $\kappa = 1.0545 \times 10^{-4}$.

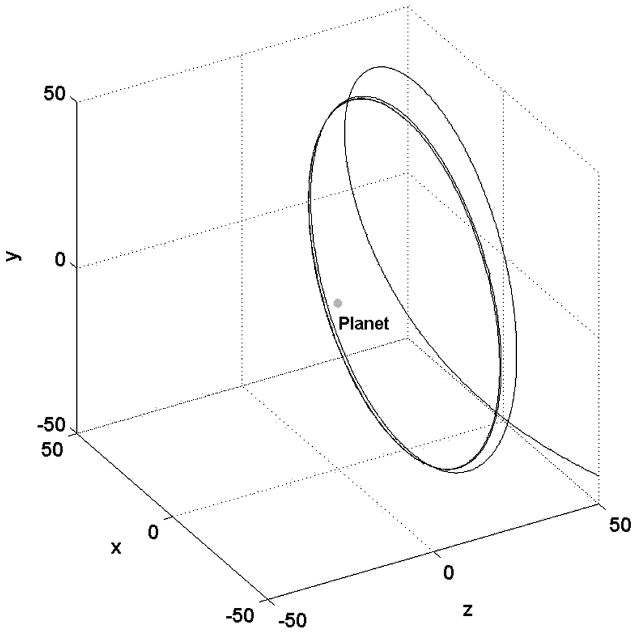

Fig. 2b Unstable displaced non-Keplerian orbit ($\rho_0 < 2\sqrt{2}z_0$): $\rho_0 = 50$ L, $z_0 = 20$ L, and $\kappa = 1.2806 \times 10^{-4}$.

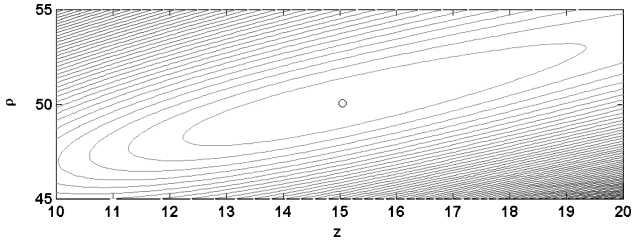

Fig. 3a Potential energy function $U(\rho_0, z_0)$ minimum at stable initial conditions ($\rho_0 > 2\sqrt{2}z_0$): $\rho_0 = 50$ L, $z_0 = 15$ L, and $\kappa = 1.0545 \times 10^{-4}$.

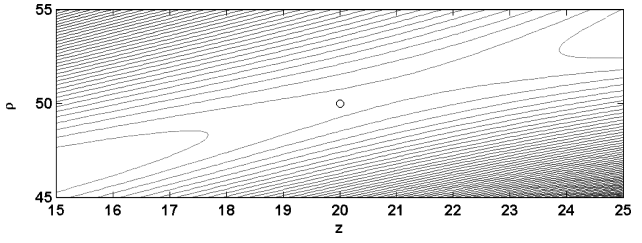

Fig. 3b Potential energy function $U(\rho_0, z_0)$ saddle point at unstable initial conditions ($\rho_0 < 2\sqrt{2}z_0$): $\rho_0 = 50$ L, $z_0 = 20$ L, and $\kappa = 1.2806 \times 10^{-4}$.

A stable orbit corresponds to a local minimum in this potential energy function, which occurs when $U_{\rho\rho} > 0$, $U_{zz} > 0$, and $U_{\rho\rho}U_{zz} - U_{\rho z}^2 > 0$. It can be demonstrated that $U_{\rho\rho} > 0$ is always true and $U_{zz} > 0$ while $\rho_0 > \sqrt{2}z_0$. An unstable orbit corresponds to a local maximum or saddle point of the potential energy function. The second derivatives are given by

$$U_{\rho\rho} = 3h_z^2/\rho_0^4 + 1/r_0^3 - 3\rho_0^2/r_0^5 \tag{11a}$$

$$U_{zz} = 1/r_0^3 - 3z_0^2/r_0^5 \tag{11b}$$

$$U_{\rho z} = -3\rho_0 z_0/r_0^5 = U_{z\rho} \tag{11c}$$

Using these derivatives and the conditions defined for a local minimum, the resulting stability condition can be reduced to $\rho_0 > 2\sqrt{2}z_0$, which demonstrates that the linear stability condition agrees with the nonlinear stability condition. Figure 3a shows the potential energy function for a stable orbit with a minimum of the function at the nominal orbit conditions. Figure 3b shows the potential energy

function of an unstable orbit, where the saddle point present at the nominal orbit conditions indicates the solar sail can escape.

Zero-Velocity Surfaces

The total energy of the orbit is now used to identify regions of trapped motion. Because total energy is conserved ($\mathrm{d}H/\mathrm{d}t = 0$), the orbit energy can be determined from the initial conditions as

$$E_0 = \tfrac{1}{2}\left(\dot{\rho}_0^2 + \dot{z}_0^2 + h_z^2/\rho_0^2\right) - 1/r_0 - \kappa z_0 \tag{12}$$

Consider now bound motion in the ρ–z plane with the definition $v^2 = \dot{\rho}^2 + \dot{z}^2$. For allowed motion v is real, and so $v^2 > 0$. Then, using the pseudopotential, Eq. (10), it is possible to test when this condition is true using

$$\tfrac{1}{2}v^2 = E_0(\rho_0, z_0) - U(\rho, z) > 0 \tag{13}$$

Figure 4a shows a zero-velocity surface bounding the motion of a solar sail. Regions of allowed motion are indicated by the shaded area, and regions of forbidden motion are represented by the lighter area. It is clear that this orbit is stable because the solar sail is trapped in a region of allowed motion separated from the open region, which extends to infinity. Figure 4b shows an unstable orbit where the solar sail is free to escape from the nominal orbit.

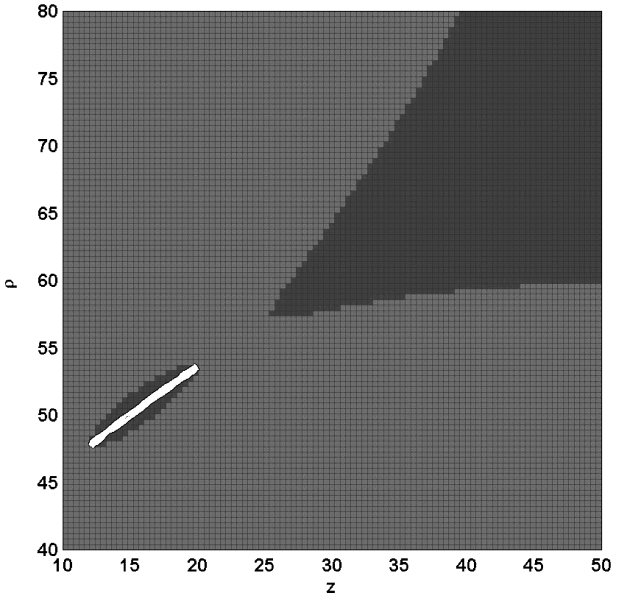

Fig. 4a Stable orbit bound within region of allowed motion ($\rho_0 > 2\sqrt{2}z_0$): $\rho_0 = 50\ L$, $z_0 = 15\ L$, and $\kappa = 1.0545 \times 10^{-4}$ (light region, forbidden motion and dark region, allowed motion).

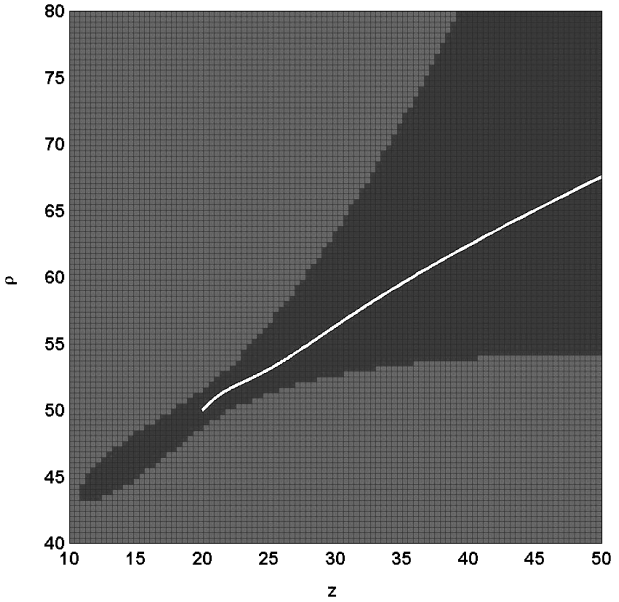

Fig. 4b Unstable orbit resulting in solar-sail escape ($\rho_0 < 2\sqrt{2}z_0$): $\rho_0 = 50\ L$, $z_0 = 20\ L$, and $\kappa = 1.2806 \times 10^{-4}$ (light region, forbidden motion and dark region, allowed motion).

Two-Body Closed-Form Solution

Hamiltonian Transformation

Euler first identified a closed-form solution to the classical two-body problem with a uniform axial force using parabolic coordinates.[19] A similar solution can be derived to include the solar radiation pressure effects introduced by the solar sail. The transformation between polar coordinates (ρ, z) and parabolic coordinates (ξ, η) is defined by $\rho = \xi\eta$ and $z = \frac{1}{2}(\xi^2 - \eta^2)$ with the time derivatives of ρ and z defined by

$$\dot{\rho} = \dot{\xi}\eta + \dot{\eta}\xi \tag{14a}$$

$$\dot{z} = \dot{\xi}\xi - \dot{\eta}\eta \tag{14b}$$

and the radial distance of the solar sail from the central body given by $r = \frac{1}{2}(\xi^2 + \eta^2)$. This allows the Hamiltonian to be written in the form

$$H(\xi, \eta) = [1/2(\xi^2 + \eta^2)]\left[P_\xi^2 + P_\eta^2 + P_\theta^2(1/\xi^2 + 1/\eta^2)\right] - 2/(\xi^2 + \eta^2) - (\kappa/2)(\xi^2 - \eta^2) \tag{15}$$

where the momenta terms P_ξ, P_η, and P_θ are defined as

$$P_\xi = \frac{\partial T}{\partial \dot{\xi}} = \dot{\xi}(\xi^2 + \eta^2) \tag{16a}$$

$$P_\eta = \frac{\partial T}{\partial \dot{\eta}} = \dot{\eta}(\xi^2 + \eta^2) \tag{16b}$$

$$P_\theta = \frac{\partial T}{\partial \dot{\theta}} = (\xi\eta)^2\dot{\theta} = \rho^2\dot{\theta} \tag{16c}$$

Equation (15) is variable separable using the Hamilton–Jacobi method.[20] A transforming function $S(t, \xi, \eta)$ is required with the form

$$S(t, \xi, \eta) = -Et + P_\theta\theta + S(\xi) + S(\eta) \tag{17}$$

where E is the total energy calculated using Eq. (12). The transforming function is chosen such that $\partial S/\partial t + H(\xi, \eta) = 0$. Using Eq. (15), the resulting expression is given by

$$-2E\xi^2 - 2E\eta^2 + P_\xi^2 + P_\eta^2 + P_\theta^2/\xi^2 + P_\theta^2/\eta^2 - 4 - \kappa(\xi^4 - \eta^4) = 0 \tag{18}$$

Equation (18) is then variable separable giving the following expressions:

$$P_\xi^2 - 2\xi^2 E - \kappa\xi^4 + P_\theta^2/\xi^2 - 4 = -\Phi \tag{19a}$$

$$P_\eta^2 - 2\eta^2 E + \kappa\eta^4 + P_\theta^2/\eta^2 = \Phi \tag{19b}$$

where Φ is the separation constant. Rearranging to solve for momenta terms P_ξ and P_η, the following bicubic polynomials are obtained:

$$P_\xi = (\sqrt{\kappa}/\xi)\left\{\xi^6 + (2E/\kappa)\xi^4 + [(4 - \Phi)/\kappa]\xi^2 - P_\theta^2/\kappa\right\}^{\frac{1}{2}} \tag{20a}$$

$$P_\eta = (\sqrt{\kappa}/\eta)\left[-\eta^6 + (2E/\kappa)\eta^4 + (\Phi/\kappa)\eta^2 - P_\theta^2/\kappa\right]^{\frac{1}{2}} \tag{20b}$$

For a given set of initial conditions, the constants E, P_θ, and Φ can be evaluated. Setting the momenta terms P_ξ and P_η equal to zero, Eq. (19) can be solved to find values of ξ and η, which correspond to constraining parabolic surfaces.

Figure 5a represents a displaced circular orbit, which is clearly bound between two parabolic surfaces. The parabolas are rotated

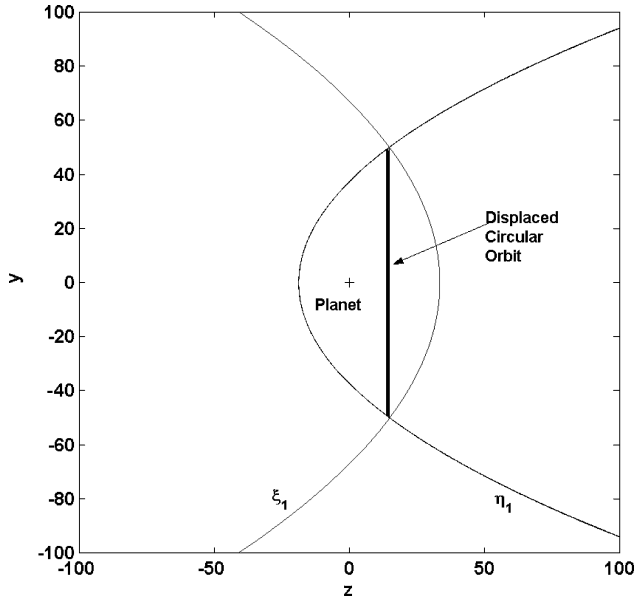

Fig. 5a Stable orbit bound between parabolic surfaces ξ_1 and η_1: $\rho_0 = 50\ L$, $z_0 = 15\ L$, and $\kappa = 1.0545 \times 10^{-4}$.

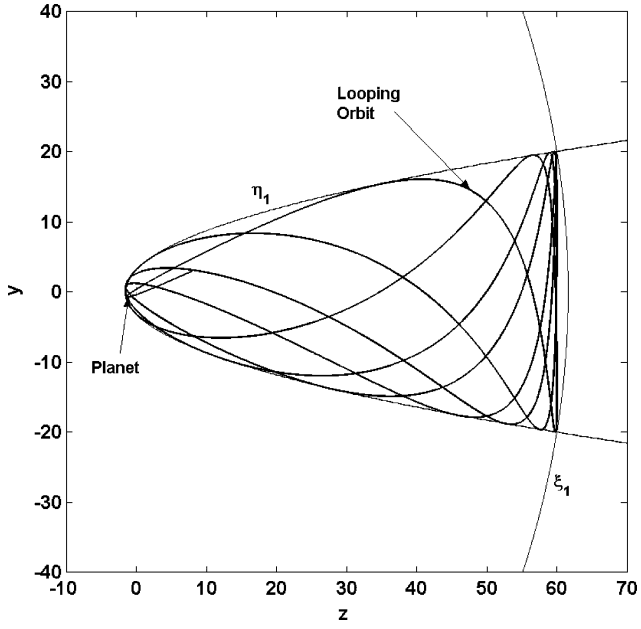

Fig. 5b Periodic looping orbit bound to paraboloid surface η_1 and constrained by ξ_1: $\rho_0 = 20\ L$, $z_0 = 60\ L$, and $\kappa = 2.3480 \times 10^{-4}$.

about the z axis (sun line) producing a paraboloid. However, Fig. 5b represents a paraboloid surface resulting from a small perturbation applied to the sail acceleration. In this case, the solar sail performs a periodic loop around the central body before returning to the nominal orbit. The closest approach distance to the central body can be determined by the point of intersection of the bounding surfaces. Once the closest distance of approach has been determined, conservation of energy can be used to calculate the initial insertion conditions from the central body to the displaced orbit.

Figure 5c uses the closed-form solution to calculate the closest approach distance to the central body for a range of nominal orbit conditions. Stable orbits, defined by $\rho_0 > 2\sqrt{2}z_0$, only experience a small displacement from the nominal orbit when sail acceleration is perturbed. Clearly unstable orbits experience much greater displacement from the nominal orbit for a small acceleration perturbation. The greater the instability of the initial orbit, the nearer to the central body the highly perturbed trajectory will pass. Useful

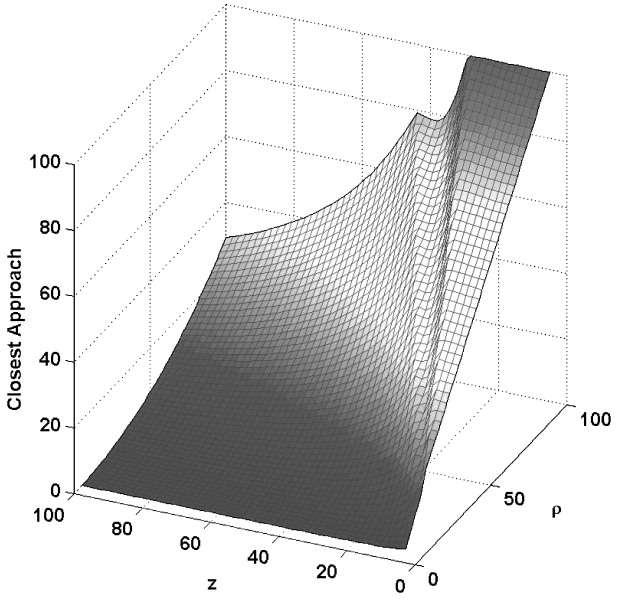

Fig. 5c Closest trajectory approach to the central body for a small acceleration perturbation(1%).

manifolds, which allow orbit insertion from near the central body, therefore require highly unstable displaced orbits, and stationkeeping techniques are necessary to prevent the solar sail escaping the desired orbit after insertion.

Periodic Looping Orbits

Demonstrated with the closed-form solution, applying a small perturbation to the nominal sail acceleration generates a new family of highly perturbed periodic orbits, defined by nested parabolae. The resulting trajectory winds off the nominal displaced orbit, then performs a pass near the central body before returning to the nominal orbit. This new family of orbits essentially provides a set of invariant manifolds.[21,22] The reduced Δv transfers offered by invariant manifolds have been taken advantage of in several missions that use the heteroclinic reconnection between the L_1 and L_2 Lagrange points.[23–25] Figure 6a shows a periodic looping trajectory that passes within 1.71 L of the central body. Figure 6b shows the periodic looping orbit trapped within a zero-velocity surface. Although the solar sail is free to move between the central body and the nominal orbit, it does not have sufficient energy to escape beyond the normal orbit displacement distance.

Non-Keplerian Orbit Control

Linear Control

A linear controller that controls the solar-sail acceleration by trimming either the sail area or sail pitch angle can be designed. Trims to the solar-sail area can be applied by using small reflective tip vanes, while trims to the sail pitch angle can be made by torquing the sail with tip vanes or mass shifts. Using the linearized equations of motion (5), a state vector $x = [\rho, z, \dot{\rho}, \dot{z}]^T$ is used to define the controller dynamics in matrix form as

$$A = \begin{bmatrix} 0 & 0 & 1 & 0 \\ 0 & 0 & 0 & 1 \\ \dfrac{\partial f_\rho}{\partial \rho} & \dfrac{\partial f_\rho}{\partial z} & 0 & 0 \\ \dfrac{\partial f_z}{\partial \rho} & \dfrac{\partial f_z}{\partial z} & 0 & 0 \end{bmatrix} \qquad B = \begin{bmatrix} 0 \\ 0 \\ \dfrac{\partial a_\rho}{\partial \chi} \\ \dfrac{\partial a_z}{\partial \chi} \end{bmatrix}$$

$$C = \begin{bmatrix} 1 & 0 & 0 & 0 \\ 0 & 1 & 0 & 0 \\ 0 & 0 & 1 & 0 \\ 0 & 0 & 0 & 1 \end{bmatrix} \qquad \begin{aligned} \dot{\boldsymbol{x}} &= A\boldsymbol{x} + B\boldsymbol{u} \\ \boldsymbol{y} &= C\boldsymbol{x} \end{aligned} \tag{21}$$

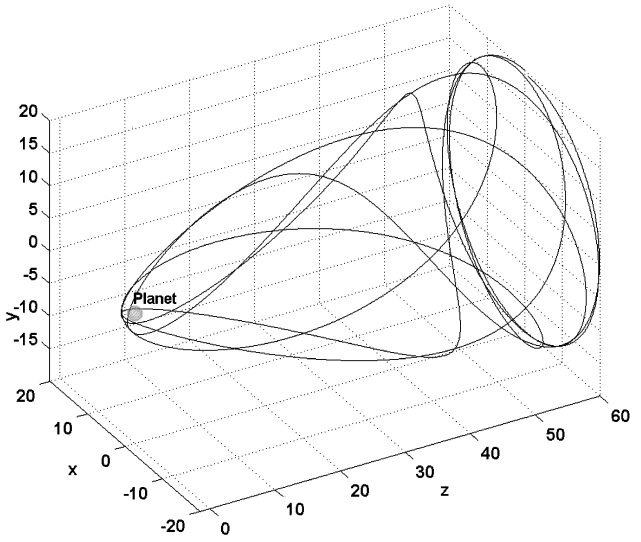

Fig. 6a Periodic looping trajectory with 1% acceleration reduction: $\rho_0 = 20\ L$, $z_0 = 60\ L$, and $\kappa = 2.3480 \times 10^{-4}$.

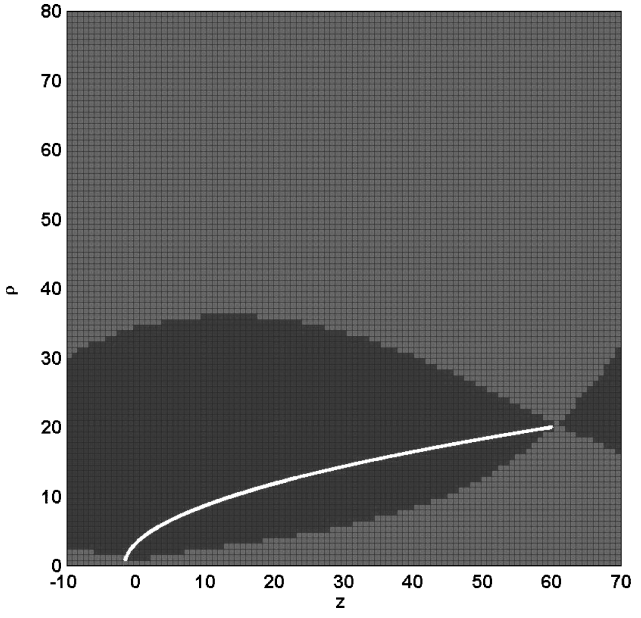

Fig. 6b Periodic looping trajectory trapped within a zero-velocity surface: $\rho_0 = 20\ L$, $z_0 = 60\ L$, and $\kappa = 2.3480 \times 10^{-4}$ (light region, forbidden motion and dark region, allowed motion).

where A is the constant coefficient system matrix, $\boldsymbol{y}$ is the output vector, $\boldsymbol{u}$ is the control vector, and $\boldsymbol{x}$ is the state-space vector.[26,27] The constant coefficient matrix A is constructed using the linearized equations of motion from Eq. (5), where the partial derivatives $\partial f_\rho/\partial\rho$, $\partial f_\rho/\partial z$, $\partial f_z/\partial\rho$, and $\partial f_z/\partial z$ are evaluated at the nominal orbit and are defined by Eq. (6). The matrix B represents the control input matrix, where variable χ epresents the control parameter (sail area or sail pitch).

The acceleration components will be represented along the ρ axis as a_ρ and along the z axis as a_z. Consider using sail area variation as the control. From Eq. (1)

$$a_\rho = \kappa \cos^2\alpha \sin\alpha \tag{22a}$$

$$a_z = \kappa \cos^3\alpha \tag{22b}$$

where κ is the nominal sail acceleration when $\alpha = 0$. Because κ varies linearly with sail area, the derivatives of the acceleration components can be written as

$$\frac{\partial a_\rho}{\partial \kappa} = \cos^2\alpha \sin\alpha = 0 \qquad (\alpha = 0) \tag{23a}$$

$$\frac{\partial a_z}{\partial \kappa} = \cos^3\alpha = 1 \qquad (\alpha = 0) \tag{23b}$$

Area control directly affects the velocity $\dot{z}$, which leads to the control matrix $B = [0\ \ 0\ \ 0\ \ 1]^T$. Similarly, for pitch-angle control the rate of change of acceleration with respect to the sail pitch angle is

$$\frac{\partial a_\rho}{\partial \alpha} = \kappa \cos^3\alpha(1 - 2\tan^2\alpha) \tag{24a}$$

$$\frac{\partial a_z}{\partial \alpha} = -3\kappa \cos^2\alpha \sin\alpha \tag{24b}$$

so that the control in this case is written in the form $B = [0\ \ 0\ \ \kappa\ \ 0]^T$, where $\alpha = 0$ on the nominal orbit. Pitch-angle variation directly affects the velocity $\dot{\rho}$, which leads to the given matrix B. The controllability matrix and observability matrix can be examined to ensure both methods provide full control of the system.

The controllability matrix M_c and observability matrix M_o are defined as

$$M_c = [B \quad AB \quad A^2B \quad A^3B] \tag{25a}$$

$$M_o = [C^T \quad A^TC^T \quad (A^T)^2C^T \quad (A^T)^3C^T] \tag{25b}$$

where the output matrix C is a 4×4 identity matrix. For a system to be fully controllable, the controllability matrix must be full rank (in this case rank 4). A completely controllable system can transfer any initial state $\boldsymbol{x}(t_0)$ to any final state $\boldsymbol{x}(t_f)$ via the control signal $\boldsymbol{u}(t)$. A system can be described as fully observable if the observability matrix is full rank. A fully observable system enables every initial state $\boldsymbol{x}(t_0)$ to be determined from the output $\boldsymbol{y}(t)$, so that $\boldsymbol{y}(t)$ is dependent on every state $\boldsymbol{x}(t)$ (Ref. 28). Both solar-sail area control and pitch-angle control obtain full-rank controllability and observability matrices. Control of the orbits is achieved using a set of gains (G_1, G_2, G_3, G_4). For solar-sail area control, the required acceleration variation is equivalent to

$$\delta\kappa = G_1(\rho - \rho_0) + G_2(z - z_0) + G_3(\dot{\rho} - \dot{\rho}_0) + G_4(\dot{z} - \dot{z}_0) \tag{26a}$$

where ρ, z, $\dot{\rho}$, $\dot{z}$ are the integrated orbit conditions and ρ_0, z_0, $\dot{\rho}_0$, $\dot{z}_0$ are the desired orbit conditions. Similarly, the pitch-angle variation can be calculated using

$$\delta\alpha = G_1(\rho - \rho_0) + G_2(z - z_0) + G_3(\dot{\rho} - \dot{\rho}_0) + G_4(\dot{z} - \dot{z}_0) \tag{26b}$$

where $\delta\alpha$ is used to calculate the resultant z- and ρ-axis accelerations using Eq. (22). In both cases the gains can be selected using either root-locus methods or later an optimal quadratic regulator.

Orbit Insertion by Using Linear Control

A solar sail can be inserted onto a non-Keplerian orbit from near the central body and linear control applied to prevent escape. To demonstrate this, consider insertion to an orbit with conditions $\rho_0 = 20\ L$ and $z_0 = 60\ L$. The parabolic bounding surfaces for the family of orbits that wind onto this orbit are provided in Fig. 5b. The closest approach distance to the central body is $1.72\ L$, determined from the intersection of the parabolae $\xi = 0.4189$ and $\eta = 1.8060$. The corresponding polar coordinate values at this point are $\rho = 0.7566\ L$ and $z = -1.5431\ L$. For the two-body case, angular momentum is conserved, and so the insertion orbit angular velocity can be calculated. Because the intersection values of z and ρ are minimum turning values along the z and ρ axis, assume that $\dot{z} = \dot{\rho} = 0$. The initial conditions are symmetric around the sun line, and so the initial angular position can be chosen arbitrarily.

Figure 7a shows orbit insertion from the calculated point without linear control. When the solar sail arrives at the nominal orbit, the small acceleration perturbation is removed. In this case, the solar sail

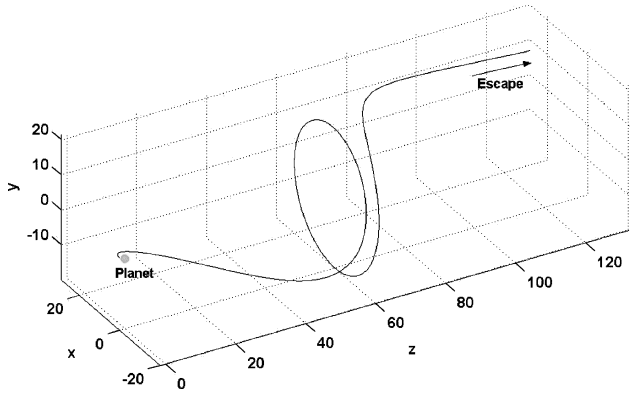

Fig. 7a Uncontrolled non-Keplerian orbit with near-planet insertion.

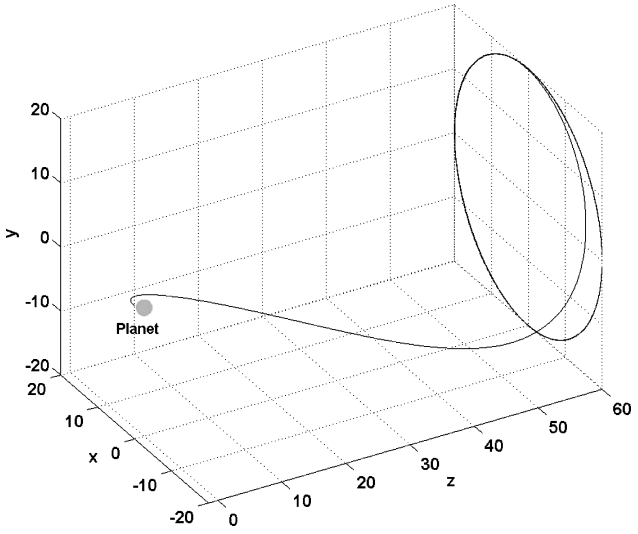

Fig. 7b Solar-sail area controlled orbit after near-planet insertion: $\rho_0 = 20\ L$, $z_0 = 60\ L$, $\kappa = 2.3480 \times 10^{-5}$, and $G = [3.12 \times 10^{-5}\quad 7.59 \times 10^{-5}\quad 1 \times 10^{-4}\quad 5 \times 10^{-4}]$.

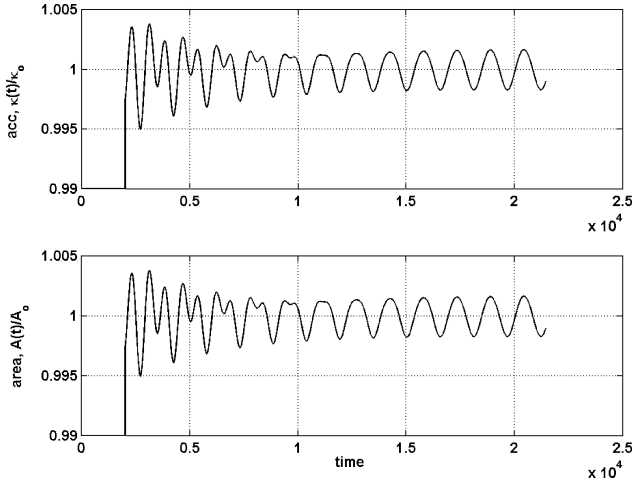

Fig. 7c Control area variation and resultant acceleration variation against nondimensionalized time. Area $A(t)$ and acceleration $\kappa(t)$ variation are represented as ratios relative to the nominal values A_0, κ_0.

escapes the desired orbit in the anti-Sun direction. Figure 7b shows a controlled non-Keplerian orbit after insertion from close to the central body. The gains were selected using the root-locus method to suppress the positive real eigenvalues. The nondimensionalized sail area and resulting acceleration variation required to control the orbit is provided in Fig. 7c.

Figure 8a shows a non-Keplerian orbit controlled using sail pitch-angle variation. Figure 8b shows the resulting acceleration variation

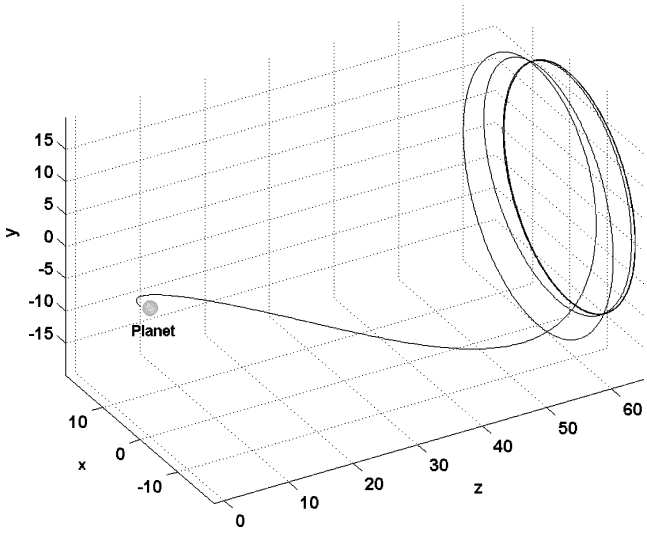

Fig. 8a Solar-sail pitch-angle controlled orbit after near-planet insertion: $\rho_0 = 20\ L$, $z_0 = 60\ L$, $\kappa = 2.3480 \times 10^{-4}$, and $G = [0.2\quad 0.15\quad 49.1\quad 100]$.

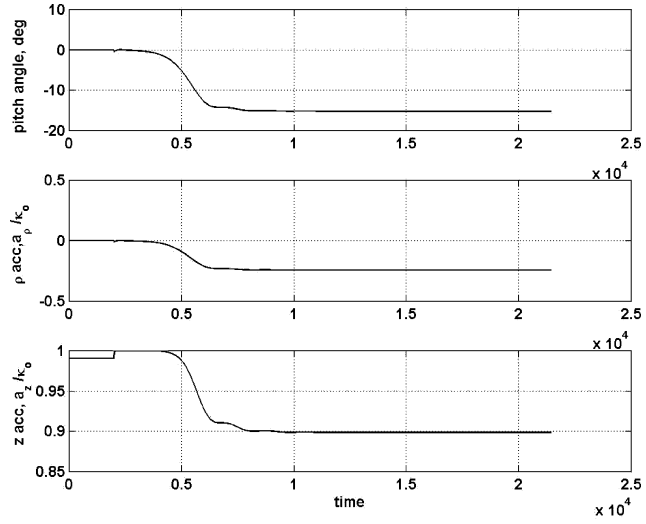

Fig. 8b Controlled pitch-angle variation and resultant acceleration variation directed along the ρ and z axes. Acceleration represented as a ratio of the nominal value κ_0.

along the ρ and z axes as a result of the actuation of the pitch angle. It is evident that the solar-sail orbit is stabilized at a displacement distance of 65 L. This is slightly further than the desired 60 L displacement and highlights one problem with the best-estimate gains selected using root-locus methods. Selecting the optimal gains using a linear-quadratic-regulator method enables the deviation from the nominal orbit and the size of actuator response to be minimized. This optimal gain selection will be adopted for orbit control within the three-body system.

Hill's Equations

A more accurate model of the dynamics of a displaced non-Keplerian orbit can be obtained using Hill's approximation to the circular restricted three-body problem. This model includes solar gravitational tide terms and the centripetal and coriolis terms due to the central body orbiting the sun. A rotating frame of reference is chosen relative to the central body. In Hill's model, the central body is assumed to have a perfectly circular motion around the sun, with the sunline parallel to the x axis and with equations represented in Cartesian form[11]

$$\ddot{x} - 2\Omega\dot{y} = -x/r^3 + 3\Omega^2 x + \kappa(t) \tag{27a}$$

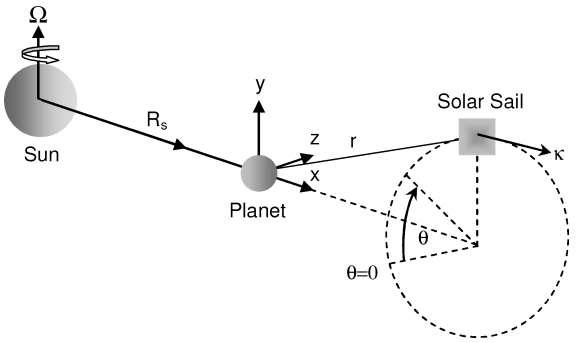

Fig. 9 Schematic representing Hill's approximation of the circular restricted three-body problem.

$$\ddot{y} + 2\Omega\dot{x} = -y/r^3 \tag{27b}$$

$$\ddot{z} = -z/r^3 - \Omega^2 z \tag{27c}$$

where the distance of the solar sail from the planet is defined as $r = \sqrt{(x^2 + y^2 + z^2)}$ and r_0 represents the distance evaluated at the nominal displaced orbit. The equations are again nondimensionalized with characteristic length $L = 1$ (central body radius) and characteristic time $\tau = \sqrt{(L^3/\mu)}$, where μ is the central body gravitational parameter. The nondimensionalized angular velocity of the central body revolving around the sun $\Omega = \sqrt{(L^3\mu_s/\mu R_s^3)}$, where μ_s is the solar gravitational parameter and R_S is the distance between the planet and the sun. A schematic of a displaced non-Keplerian orbit is provided in Fig. 9.

Another factor to be included in Hill's equations is the variation of the acceleration due to solar radiation pressure. The inverse square dependency of acceleration due to solar radiation pressure introduces a small variation from the nominal value required to displace the solar sail a desired distance from the central body. The distance between the sun and the solar sail at the nominal orbit is equivalent to $R_0 = |R_S + r_0|$ and the instantaneous distance $R(t) = |R_S + r(t)|$. The acceleration due to solar radiation pressure at any distance from the planet is therefore equivalent to $\kappa(t) = [R_0/R(t)]^2\kappa_0$, where the acceleration calculated at the nominal orbit $\kappa_0 = x_0/r^3 - 3\Omega^2 x_0$, from Eq. (27a).

Optimal Linear Control

Optimal control laws can be applied to help select gains that use sail area or pitch-angle control for stationkeeping. Treating the three-body problem as a perturbed two-body problem, the linear controller represented by Eq. (21) can be adapted for control of non-Keplerian orbits using Hill's equations. Optimal control is necessary in the three-body problem to dampen the effects of periodic perturbations. Optimal control theory provides a method for selecting a gain matrix that suppresses any unstable eigenvalues based on a cost function V

$$V = \int_t^\infty [\boldsymbol{x}'(\tau)Q\boldsymbol{x}(\tau) + \boldsymbol{u}'(\tau)N\boldsymbol{u}(\tau)]\,\mathrm{d}\tau \tag{28}$$

where t is the initial integration time. The first term inside the brackets represents the penalty on the deviation of state vector $\boldsymbol{x}$ from the nominal orbit conditions, and the second term represents the cost of control, which limits the size of the control signal. The aim is to select a gain matrix G that minimizes the performance function V. This can be achieved using the Ricatti equation

$$-\dot{M} = MA + A'M - MBN^{-1}B'M + Q \tag{29}$$

where M is the performance matrix and is related to the performance function such that $V = x'Mx$. Provided that M converges to a limit as $t \to \infty$, it can be assumed that $\dot{M} \to 0$. Equation (29) can be solved for M, which enables the optimal gain matrix to be calculated using $G = N^{-1}B'M$ (Ref. 29).

Optimal Solar-Sail Area Control

Optimal solar-sail area control will be demonstrated by controlling a non-Keplerian orbit of radius 20 L displaced 60 L in the antisun direction. The solar sail is delivered to this non-Keplerian orbit via a near-planet insertion using the family of winding orbits. The gain matrix was selected using the two-body equations, as suggested earlier. The state weighting and control weighting matrix were selected using an initial guess, which was gradually improved to provide a good level of control for a reasonable control signal size. Figure 10a shows the controlled orbit, where the state error is calculated using polar coordinates. The Cartesian coordinates are converted to polar using $\rho = \sqrt{(y^2 + z^2)}$ and $\dot{\rho} = (y\dot{y} + z\dot{z})/\rho$ after each integration step, which are then compared to the nominal orbit conditions $\rho_0 = 20\,L$, $z_0 = 60\,L$, $\dot{\rho}_0 = 0$, $\dot{z}_0 = 0$. The acceleration variation is calculated using Eq. 26a, where the resultant acceleration directed along the sun line is equivalent to $\kappa(t) + \delta\kappa(t)$. Figure 10b shows the required area and acceleration variation to prevent the solar sail escaping the nominal orbit after insertion. The acceleration is normalized as the ratio of the control acceleration relative to the nominal value $\kappa(t)/\kappa_0$. Similarly, the area is normalized as the ratio of controlled sail area to the nominal area $A(t)/A_0$. It is clear that

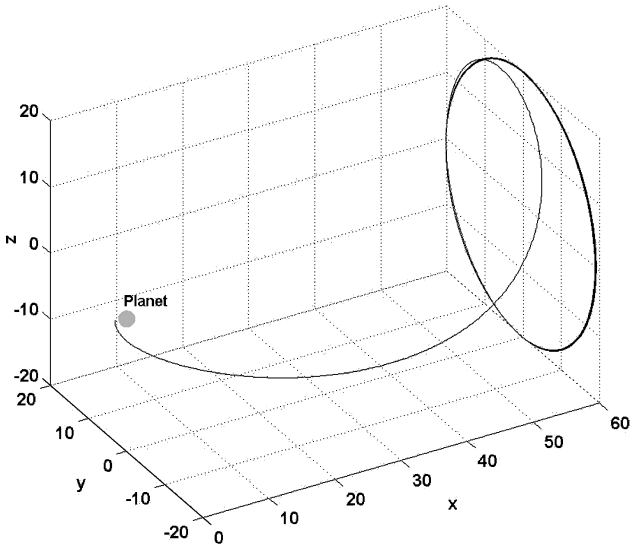

Fig. 10a Linear sail area controller activated on arrival at the nominal orbit: $\rho_0 = 60\ L$, $z_0 = 20\ L$, $Q = 1000\,(I_{4\times4})$, $N = 3 \times 10^{11}$, and $G = [-3.0769 \times 10^{-5}\ \ 7.4970 \times 10^{-5}\ \ 0.012174\ \ 0.012245]$.

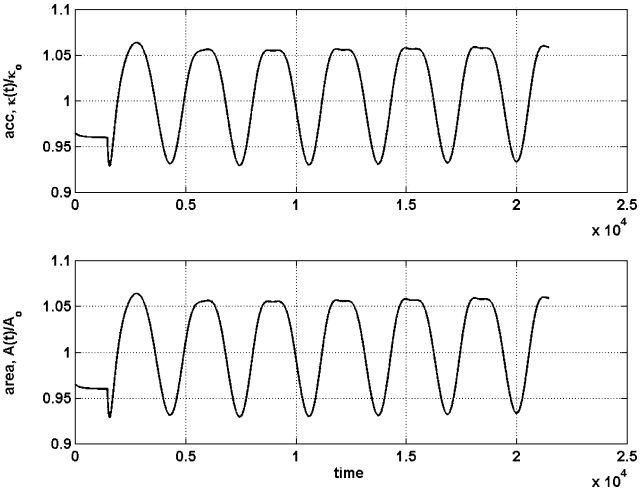

Fig. 10b Control area variation and resultant acceleration variation against nondimensionalized time. Area $A(t)$ and acceleration $\kappa(t)$ variation are represented as ratios relative to the nominal calculated values A_0, κ_0.

the area variation is smooth and periodic, which avoids the technical difficulties of large, rapid sail area variations over a short period of time.

Optimal Pitch- and Yaw-Angle Control

Solar-sail orbit control can also be achieved by varying the sail pitch and yaw angle. A similar controller is designed based on the two-body polar equations. The required pitch-angle variation is calculated using Eq. (26b), where the initial pitch angle $\alpha_0 = 0$. As Hill's equations are derived using Cartesian coordinates, it is necessary to convert the polar pitch angle α and the polar angular position θ into a Cartesian pitch angle ψ and a Cartesian yaw angle ϕ. The conversion between the polar and Cartesian angles is achieved using the following equations:

$$\psi = \sin^{-1}(\sin\alpha\cos\theta) \tag{30a}$$

$$\phi = \tan^{-1}(\tan\alpha\sin\theta) \tag{30b}$$

where $\theta = \tan^{-1}(y/z)$. The acceleration components (a_x, a_y, a_z) can then be calculated by converting Eq. (21) into Cartesian form using the pitch and yaw angles (ϕ, ψ) as

$$a_x = \kappa(t)\cos^3\psi\cos^3\phi \tag{31a}$$

$$a_y = \kappa(t)\cos^3\psi\cos^2\phi\sin\phi \tag{31b}$$

$$a_z = \kappa(t)\cos^2\psi\cos^2\phi\sin\psi \tag{31c}$$

where $\kappa(t)$ includes the inverse square acceleration dependency as the distance from the sun varies.

Figure 11a shows a controlled orbit with nominal conditions $z_0 = 20\ L$ and $x_0 = 60\ L$ after insertion at 1.546 L from the central body. When the controller is activated, the sail acceleration is raised to 1.05 κ_0. The increased acceleration is necessary as the maximum acceleration along the sun line occurs when the pitch angle $\alpha = 0$. If the solar sail moves toward the central body, it is necessary to increase the acceleration above the nominal value to drive the solar sail back toward the nominal orbit. This also imposes an upper pitch-angle limit, which can be limited using the cost of control matrix N.

Figure 11b shows the sail pitch- and yaw-angle variation required to control the orbit after insertion. The optimized gains result in a periodic control, which is used to dampen the periodic perturbations intrinsic with Hill's equations.

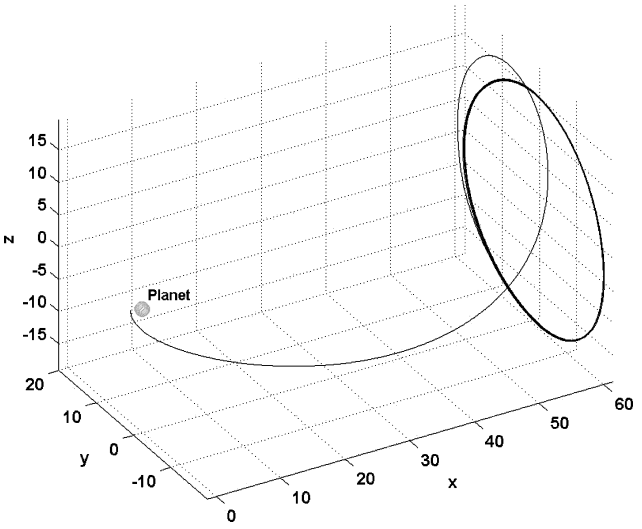

Fig. 11a Linear pitch-angle controller activated on arrival at the nominal orbit. Acceleration increased to 1.05 κ on arrival at the nominal orbit: $\rho_0 = 60\ L$, $z_0 = 20\ L$, $Q = 1000\,(I_{4\times4})$, $N = 1 \times 10^{-4}$, and $G = [0.2291\ \ 0.8056\ \ 42.8928\ \ 302.7755]$.

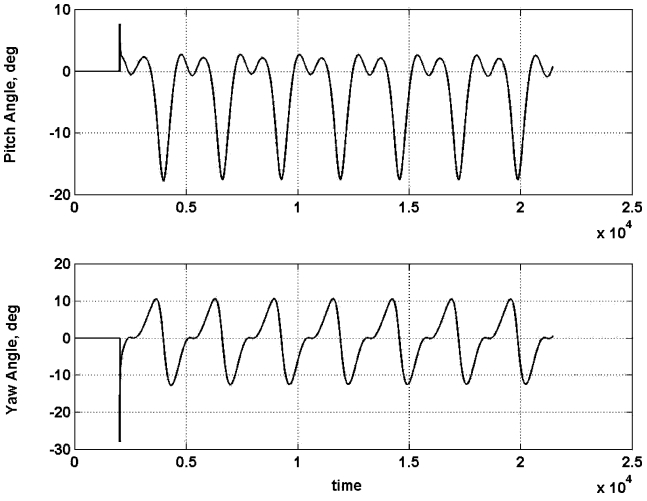

Fig. 11b Required pitch- and yaw-angle variation to prevent the solar sail from escaping the nominal orbit.

Non-Keplerian Orbit Within the Geomagnetic Tail

Nominal Orbit

A solar sail could be used to position a science payload within the Earth's magnetic tail. By inserting the solar sail into a non-Keplerian orbit displaced 30 R_E (Earth radii) from the Earth, the processes of magnetic reconnection could be studied over a long duration. The mission would require a high-performance solar sail with mass of 400 kg to position a 100-kg science payload. A suitable nominal orbit is selected with radius 20 R_E displaced 30 R_E from the Earth. Such an orbit would require a solar-sail acceleration of 6 mms^{-2} and sail loading of 1.52 gm^{-2}. This mission would require a highly advanced solar sail with current technology enabling large-area structures with loading between 5–10 gm^{-2}. This would require advances in gossamer spacecraft technology, but with more efficient substrate coating techniques and improvements in the design of the substrate it is not infeasible.[15]

The initial insertion conditions are selected from the set orbits that wind onto the displaced non-Keplerian orbit. An acceleration perturbation is applied at 96% of the nominal acceleration, providing a set of orbits with a closest Earth approach distance of 3.39 R_E. Figure 12a shows a non-Keplerian orbit controlled using solar-sail area variation for a period of 100 days. The sail area is required to vary between 2.9383–3.6338 $\times 10^5$ m with a resultant acceleration variation between 5.3662 and 6.6363 mms^{-2} (see Fig. 12b). The required area variation is rather large, so that sail pitch and yaw control is more suitable. The largest acceleration required corresponds to a sail loading parameter of 1.38 gm^{-2}, equivalent to a disc sail configuration with a radius of 340 m. Figure 13a shows the same orbit after insertion controlled using sail pitch- and yaw-angle variations. The necessary sail angle variations are provided in Fig. 13b. Over this 100-day control period, the pitch angle varies between −13.9 and 17.4 deg; the yaw angle varies between −20.8 and 8.0 deg. Again selecting a disc sail configuration, the required radius would be 338 m with a required sail loading of 1.39 gm^{-2}.

An alternative mission could make use of the invariant manifolds to sweep out a large area of the geomagnetic tail. This would provide good spatial coverage, but there would be loss of temporal coverage. It would be difficult to obtain useful data to model accurately the dynamics of the geomagnetic tail as both the solar-sail displacement distance and the local plasma density are varying continuously. To improve temporal coverage, it would be necessary to have several solar sails collecting data simultaneously at different locations within the geomagnetic tail.

Transfer Trajectory

Inserting the solar sail onto a trajectory that winds onto the displaced orbit can be achieved using a Hohmann transfer maneuver.

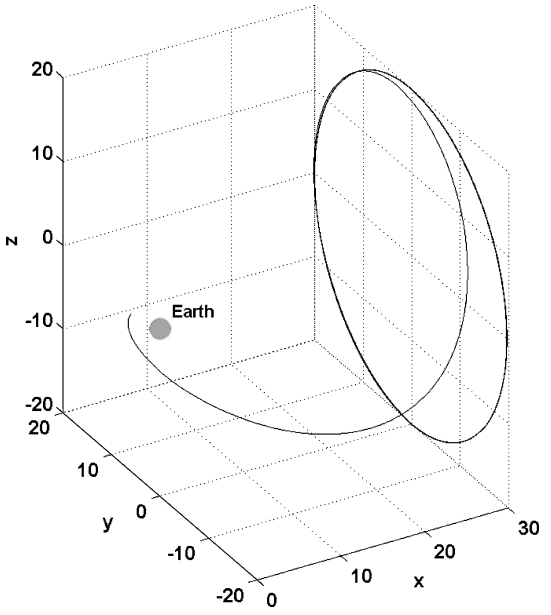

Fig. 12a Sail area variation controlling a non-Keplerian orbit within the geomagnetic tail: $\rho_0 = 20$ RE, $z_0 = 30$ RE (Earth radii), $\kappa = 6.01$ mms^{-2}, $Q = 1500\,(I_{4\times 4})$, $N = 1 \times 10^{10}$, and $G = [-1.1562 \times 10^{-4}\ \ 5.1455 \times 10^{-4}\ \ 0.044469\ \ 0.032082]$.

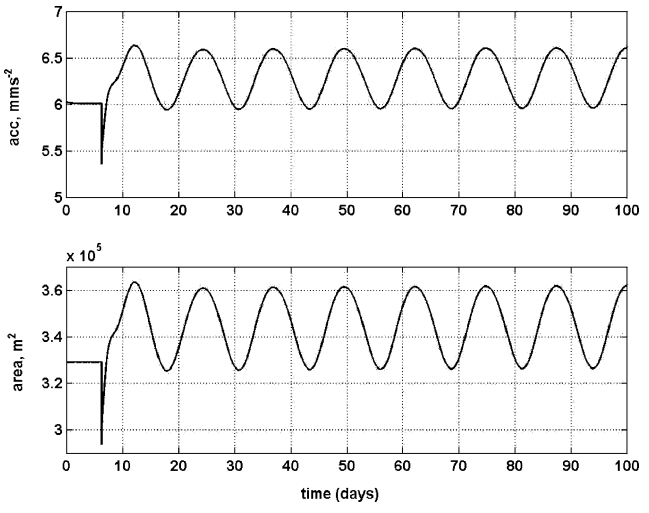

Fig. 12b Required sail area and acceleration variation to prevent escape from a non-Keplerian orbit within the geomagnetic tail.

A suitable launch vehicle to deliver the 500-kg solar sail and payload to a 200-km altitude low Earth orbit (LEO) would be the either the ESA Vega Launcher or the European/Russian Rockot Launcher; both are capable of delivering a 2000-kg payload to LEO leaving mass for the kick motors required for transfer to the insertion manifold. The orbit plane is selected so that the orbit insertion point and the center of the Earth are coplanar. The plane inclination is selected so the insertion velocity vector, directed along the z–y axis, is parallel to the Hohmann transfer second kick stage velocity. The Δv requirements for the transfer to the invariant manifold from LEO are also provided. The orbit inclination is equivalent to 40.58 deg relative to the equatorial plane. Figure 14 shows the orbit insertion stages of the Hohmann transfer performed using two kick motors. The time taken between the first and second burn is 2 h 18 min 44 s. After the final burn, the solar sail is deployed and follows the manifold of trajectories winding onto the desired orbit.

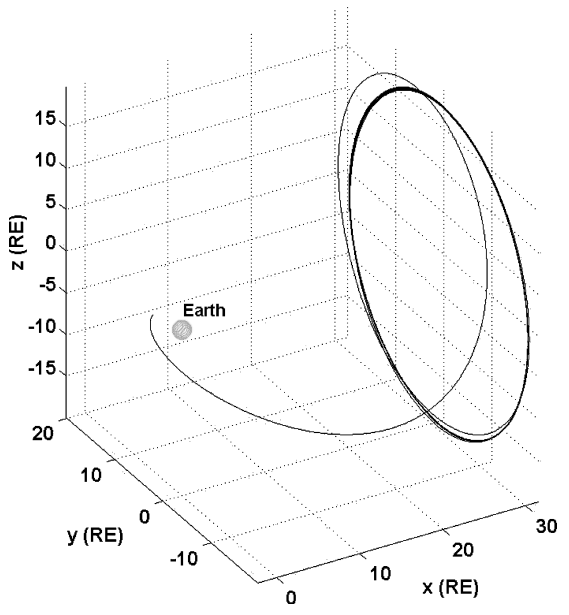

Fig. 13a Sail pitch- and yaw-angle variation controlling a non-Keplerian orbit within the geomagnetic tail: $\rho_0 = 20$ RE, $z_0 = 30$ RE (Earth radii), $Q = 100\,(I_{4\times 4})$, $N = 1 \times 10^4$, $\kappa = 6.57$ mms^{-2}, and $G = [0.2533\ \ 0.4914\ \ 27.4537\ \ 90.5139]$.

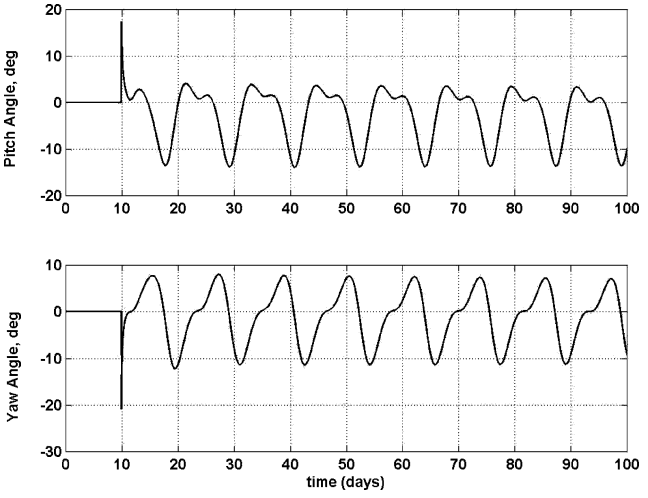

Fig. 13b Required sail pitch- and yaw-angle variation to prevent escape from a non-Keplerian orbit within the geomagnetic tail.

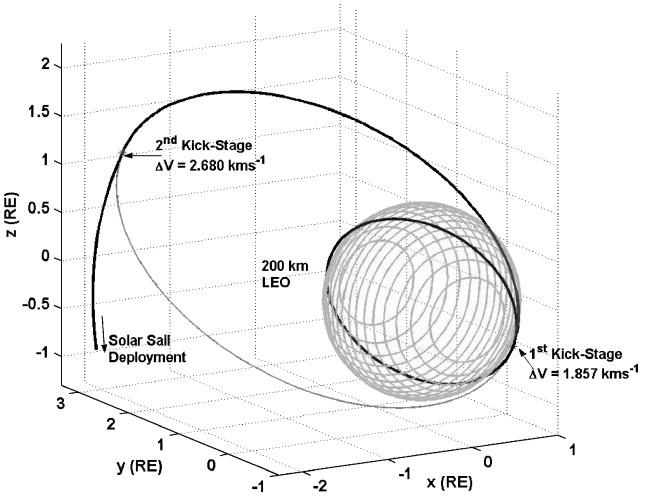

Fig. 14 Hohmann transfer from 200-km LEO to invariant manifold insertion.

Conclusions

This paper has considered the application of solar sails to generate displaced non-Keplerian orbits at planetary bodies. The stability of these orbits has been investigated using both a linear and nonlinear analysis. A closed-form solution was derived for the two-body case using parabolic coordinates and including the acceleration due to solar radiation pressure. A new family of orbits, which are mapped to the surface of bounding parabolas, was then identified. This provides families of useful orbits that wind onto the displaced non-Keplerian orbit and can be used to insert a solar sail into a non-Keplerian orbit. A linear controller was designed to prevent escape from the nominal orbit after insertion. Two possible methods for controlling the solar-sail acceleration were considered: sail area control and sail pitch-angle control. Both methods are fully controllable and observable.

Treating the three-body problem as a perturbed two-body model, an optimal controller was designed to select control gains, which minimize the sail area or pitch-angle variation required to control displaced non-Keplerian orbits. A possible mission to the geomagnetic tail was investigated where a high-performance solar sail is required to position a 100-kg payload at a displacement distance of 30 Earth radii. Launch vehicle Δv requirements were investigated where possible options include the Rockot or Vega launchers, both capable of delivering a 2000-kg payload to low Earth orbit. The use of a non-Keplerian orbit with a robust controller could enable long-duration science missions within the geomagnetic tail.

Acknowledgment

This work was carried out with part financial support from the Lockheed Martin Corporation Advanced Technology Center, Palo Alto, California.

References

[1]Dachwald, B., and Seboldt, W., "Solar Sailcraft of the First Generation—Mission Applications to Near-Earth Asteroids," International Astronautical Congress Paper 03-Q.5.06, Sept. 2003.

[2]Seboldt, W., and Dachwald, B., "Solar Sails for Near-Term Advanced Scientific Deep Space Missions," *Rocket Propulsion: Present and Future, Proceedings of the 8th International Workshop on Combustion and Propulsion*, No. 49, edited by L. T. Deluca, Politecnico di Milano, Milan, 2003.

[3]Leipold, M., Seboldt, W., Lingner, S., Borg, E., Hermann, A., Pabsch, A., Wagner, O., and Bruckner, J., "Mercury Sun-Synchronous Polar Orbiter with a Solar Sail," *Acta Astronautica*, Vol. 39, Nos. 1–4, 1996, pp. 143–151.

[4]Leipold, M., "To the Sun and Pluto with Solar Sails and Micro-Sciencecraft," *Acta Astronautica*, Vol. 45, Nos. 9–5, 1999, pp. 549–555.

[5]Hughes, G., MacDonald, M., McInnes, C., Atzei, A., and Falkner, P., "Analysis of a Solar Sail Mercury Sample Return Mission," International Astronautical Congress, Paper 04-S.2.b.08, Oct. 2004.

[6]Macdonald, M., and McInnes, C. R., "A Near-Term Roadmap for Solar Sailing," International Astronautical Congress, Paper 04-U.1.09, Oct. 2004.

[7]McInnes, C. R., McDonald, A. J. C., Simmons, J. F. L., and MacDonald, E. W., "Solar Sail Parking in Restricted Three Body Systems," *Journal of Guidance, Control, and Dynamics*, Vol. 17, No. 2, 1994, pp. 399–406.

[8]McInnes, C. R., "Artificial Lagrange Points for a Non-Perfect Solar Sail," *Journal of Guidance, Control, and Dynamics*, Vol. 22, No. 1, 1999, pp. 185–187.

[9]McInnes, C. R., "Passive Control of Displaced Solar Sail Orbits," *Journal of Guidance, Control, and Dynamics*, Vol. 21, No. 6, 1998, pp. 975–982.

[10]Forward, R. L., "Statite: A Spacecraft That Does Not Orbit," *Journal of Spacecraft and Rockets*, Vol. 28, No. 5, 1991, pp. 606–611.

[11]Morrow, E., Scheeres, D. J., and Lubin, D., "Solar Sail Orbit Operations at Asteroids," *Journal of Spacecraft and Rockets*, Vol. 38, No. 2, 2001, pp. 279–286.

[12]McInnes, C. R., and Simmons, J. F. L., "Solar Sail Halo Orbits II: Geocentric Case," *Journal of Spacecraft and Rockets*, Vol. 29, No. 4, 1992, pp. 472–479.

[13]McInnes, C. R., "Existence and Stability of Families of Displaced Two-Body Orbits," *Celestial Mechanics and Dynamical Astronomy*, Vol. 67, No. 2, 1997, pp. 167–180.

[14]Waalkens, H., Junge, A., and Dullin, H., "Quantum Monodromy in the Two-Centre Problem," *Journal of Physics A: Mathematical and General*, Vol. 36, No. 20, May 2003, pp. 307–314.

[15]McInnes, C. R., *Solar Sailing: Technology, Dynamics and Missions Applications*, Springer-Praxis Series in Space Science and Technology, Springer-Verlag, Berlin, 1999, pp. 34–40.

[16]McInnes, C. R., "Dynamics, Stability, and Control of Displaced Non-Keplerian Orbits," *Journal of Guidance, Control, and Dynamics*, Vol. 21, No. 5, 1998, pp. 799–805.

[17]McInnes, C. R., Macdonald, M., and Hughes, G., "Technical Note 10—Solar Polar Orbiter," ESA/ESTEC Contract Rept., Univ. of Glasgow, ESTEC 16534/02/NL/NR, Scotland, U.K., June 2004.

[18]Dankowicz, H., "Some Special Orbits in the Two-Body Problem with Radiation Pressure," *Journal of Celestial Mechanics and Dynamical Astronomy*, Vol. 58, No. 4, 1994, pp. 353–370.

[19]Burns, R. E., "Motion of an Artificial Satellite Under Combined Influence of Planar and Keplerian Force Fields," NASA TN D-4622, July 1968.

[20]Landau, L. D., and Lifschitz, E. M., *Mechanics—Course of Theoretical Physics*, Vol. 1, Pergamon, Oxford, 1976, pp. 151–154.

[21]Feng, B., and Rui, H., "A Survey on Homoclinic and Heteroclinic Orbits," *Applied Mathematics E-Notes*, Vol. 3, 2003, pp. 16–37.

[22]Glendinning, P., *Stability, Instability and Chaos: an Introduction to the Theory of Nonlinear Differential Equations*, Cambridge Texts in Applied Mathematics, Cambridge Univ. Press, Cambridge, U.K., 1994, pp. 77–88.

[23]Farquhar, R. W., "The Flight of ISEE-3/ICE Origins, Mission History and a Legacy," *Journal of Astronautical Sciences*, Vol. 49, No. 1, 2001, pp. 23–73.

[24]Koon, W. S., Lo, M. W., Marsden, J. E., and Ross, S. D., "Low Energy Transfer to the Moon," *Celestial Mechanics and Dynamical Astronomy*, Vol. 81, Nos. 1–2, 2001, pp. 63–73.

[25]Franz, H., Sharer, P., Ogilvie, K., and Desch, M., "WIND Nominal Mission Performance and Extended Mission Design," *Journal of Astronautical Sciences*, Vol. 49, No. 1, 2001, pp. 145–167.

[26]Marshall, S. A., *Introduction to Control Theory*, Macmillan, London, 1978, pp. 212–215.

[27]Driels, M., *Linear Control Systems Engineering*, McGraw–Hill, New York, pp. 487–492.

[28]D'Azzo, J. J., and Houpis, C. H., *Linear Control System Analysis and Design: Conventional and Modern*, 4th ed. McGraw–Hill Series in Electrical Engineering, McGraw–Hill, New York, 1995, Chap. 13, pp. 423–461.

[29]Friedland, B., *Control System Design: An Introduction to State-Space Methods*, McGraw–Hill Series in Electrical Engineering, McGraw–Hill, New York, 1986, Chap. 9, pp. 337–369.